Intern. J. Neuroscience, 2001, Vol. 107, pp. 161–171
Reprints available directly from the publisher
Photocopying permitted by license only

FREQUENCY DOMAIN EQUIVALENCE BETWEEN POTENTIALS AND CURRENTS USING LORETA

J. F. GOMEZ* and R. W. THATCHER

Bay Pines VA Medical Center, Bay Pines Foundation and the Defense and Veterans Head Injury Program (DVHIP)

(Received 25 July 2000; In final form 3 August 2000)

Analyzing the preferences of brain regions to oscillate at specific frequencies gives important functional information. Application of discrete inverse solutions for the EEG/MEG inverse problem in the frequency domain usually involves the use of many current sources (sometimes 10^4 or more) restricted to gray matter points, as the solution space for the possible generators. This number can progressively increase with the level of detail of the MRI when it is used in co-registration with EEG/MEG. However, the computation of the Fourier transform to all these sources is computationally intensive. We illustrate with a simple example how this procedure can be simplified by applying the Fourier transform to the signals in the sensors using a popular inverse method (LORETA). We also suggest how the search space of current sources at specific frequencies of oscillation can be limited to some regions constrained by other technologies such as fMRI, PET and SPECT.

Keywords: Source location; EEG/MEG inverse problem; Low resolution electromagnetic tomography; Current density

1. INTRODUCTION

The integration of the high time resolution but low spatial resolution of the EEG/MEG with the low temporal resolution but high spatial resolution of the MRI is a method to evaluate the neural network dynamics of the human brain (Toro *et al.*, 1994; Thatcher *et al.*, 1994).

*Address for correspondence: Research and Development Service–151, Veterans Administration Medical Center, Bay Pines, Florida 33744. Tel.: (727) 398-6661 Ext. 4021.

Three dimensional co-registration of the current sources of the EEG/MEG with the MRI is generically referred to as electromagnetic tomography (Pasqual-Marqui, 1994a, 1994b; Thatcher, 1995). An advantage of co-registration of EEG/MEG and MRI is that one can obtain a large number of signals directly related to information processing in populations of neurons as contrasted to blood flow measures such as PET and fMRI which detect indirect or secondary effects of neural processing. However, a limitation of the scalp recorded EEG is that volume conduction in the brain limits the spatial resolution of the 3-dimensional current sources that at any moment give rise to the electrical potentials recorded at the scalp surface (Handerson *et al.*, 1975; Thatcher *et al.*, 1977).

Recent advances in EEG source localization using forward and inverse electrodynamic solutions have improved the accuracy and spatial resolution of the source generators that give rise to the scalp recorded EEG. For example, a Laplacian smoothing of a large array of fixed location dipole sources called Low Resolution Electromagnetic Tomography (LORETA) provides an accurate 3-dimensional inverse solution with spatial resolution on the order of several centimeters (Pasqual-Marqui *et al.*, 1994a; Anderer *et al.*, 1998a). Recently, the gray matter pixels from an MRI have been used to constrain the inverse solution of LORETA and provide accurate images of EEG current sources at different frequencies within the interior of the brain (Valdez, 1997). While LORETA is an accurate low spatial resolution estimator of current source locations it is computationally complicated by the large number of source locations that are used to solve the inverse problem. Frequency analyses of the current sources in LORETA can be arduous and taxing by virtue of the large number of Fourier transforms that must be computed, three for each source gray matter point which can be several thousand (Valdes *et al.*, 1998).

An improved methodology of frequency analysis may be possible if it can be shown that there is a linear equivalence between the Fourier transform of the EEG recorded from a relatively small number of scalp sensors to the Fourier transform of current sources derived from a large number of 3-dimensional vector source points in the interior of the brain. If such a linear equivalence is present, then one needs only to compute the Fourier transform of the surface EEG and use the

Fourier coefficients to describe the frequency domain of any 3-dimensional current source in the interior of the brain without having to compute the Fourier transform for each of the interior points. Such equivalence could represent a considerable savings in effort and time.

Thus, the purpose of this paper is to explore the issue of linear frequency equivalence between the surface EEG and the 3-dimensional gray matter points inside the brain that are used in the computation of current source generators using LORETA. This will be accomplished by first deriving a mathematical expression of linear equivalence for the inverse solution of LORETA and then using simulation to demonstrate this equivalence.

2. MATHEMATICS OF LINEAR, INSTANTANEOUS, DISCRETE INVERSE SOLUTIONS

We use a linear, discrete, instantaneous forward model, within which the action of the currents J on the signals S in the sensors (electrodes or SQUIDs) can be modeled as a weighted sum of the currents:

$$\mathbf{S} = \mathbf{KJ} \tag{1}$$

where the matrix $\mathbf{K}$, representing the weights, is the lead field (Malmivuo and Plonsey, 1995). It reflects the sensitivity of the sensors to the sources and depends on the 3-dimensional coordinates, the conductivity of the tissues (bone, scalp, neural tissue) and the model used to describe the head (normally, a three shell sphere). The time domain of current sources and the time domain of scalp surface EEG are defined by one linearly equivalent time series. $\mathbf{S}$ is an $N \times W$ matrix for the scalp potentials (EEG) or the magnetic fields (MEG), or a combination of both, where N is the number of sensors and W is the number of time samples (slices). $\mathbf{J}$ is a $3M \times W$ matrix, where M is the number of sources; each source has three components parallel to the X, Y and Z axis and W being the same time samples as for $\mathbf{S}$.

For the inverse solution of (1), the currents at gray matter points are a linear combination of the signal $\mathbf{S}$ in the sensors:

$$\mathbf{J} = \mathbf{T} \cdot \mathbf{S} \tag{2}$$

where **T** is some generalized inverse of **K** (Pasqual-Marqui *et al.*, 1994). For the minimum norm solution $\mathbf{T} = (\text{pinv}(\mathbf{K}' \cdot \mathbf{K})) \cdot \mathbf{K}'$, where $\mathbf{K}'$ is the transpose of **K** · represents matrix multiplication and pinv(**X**) is the Moore-Penrouse pseudoinverse of **X** (Menke, 1984). In this paper, we use a more generalized expression to avoid the problem that the minimum norm has to localize deep sources. This method, called Low-Resolution Computed Tomography (LORETA) uses additional criteria to localize sources based in physiological considerations and consequently a Laplacian Operator is included (Pasqual-Marqui, 1994a):

$$\mathbf{T} = \{\text{inv}(\mathbf{WB}'\mathbf{BW})\}\mathbf{K}'\{\text{pinv}(\mathbf{K}\ \text{inv}(\mathbf{WB}'\mathbf{BW})\mathbf{K}'\} \tag{3}$$

where **B** is the discrete Laplacian Operator and **W** is a weighting matrix (inv indicates inverse).

The fast Fourier transform or **FFT** is a linear operator such that for any inverse solution of the form (2):

$$\text{FFT}(\mathbf{J}) = \text{FFT}[\mathbf{T} \cdot \mathbf{S}] = \mathbf{T} \cdot \text{FFT}[\mathbf{S}] \tag{4}$$

This short-hand notation shows that mathematically the same equivalence can be used to calculate the T matrix for all dipole source localization methods, *e.g.*, minimum norm, LORETA, *etc.* (Baillet, 1997). Consequently, the Fourier transform of the currents can be obtained easily by first computing the FFT of the signals in the sensors and then multiplying the **T** weights by the scalp derived FFT coefficients. This linear equivalence greatly simplifies the computation of the frequency analysis of the 3-dimensional current sources, since the application of the FFT to the sources involves 3M FFTs. In some models, the number of gray matter points is 700 and can be as high as 20000. The reduction in computation time can be 3 M/N or about two orders of magnitude (10^2).

3. SIMULATIONS OF SENSOR *VERSUS* SOURCE FOURIER TRANSFORMS USING LORETA

In our simulation we used four sensors ($N = 4$) and eight interior current source density points ($M = 8$), four of them immediately below

the sensors where gray matter regions exist. These four points are the equivalent sources of all the close generators that produce a signal in that sensor. The other points account for the other generators located far from them. A conventional spherical head model was calculated from algorithms based on MRI scanning of electrode location using markers (Lagerlud *et al.*, 1993). In the simulations, the coordinates of the electrodes corresponded to the best-fitting sphere relative to cortical anatomy (Towle *et al.*, 1993). The origin of the coordinate system was in the center of the sphere which coincides with the floor of the third ventricle 5 mm anterior to the posterior commissure (*i.e.*, the "Descartes's point", Towel *et al.*, 1993). Because the location variability due to the head shape is greatest in the temporal region (Towle *et al.*, 1993) we chose only occipital and frontal sensors located in the positions F7, F8, O1 and O2. These sensors are located in the same z-plane ($z=0$). Besides, in these regions, the geometry of the head is more close to a spherical wedge. The optimal radio of the sphere that best fit the anatomy is 8.8 cm (Towel *et al.*, 1993) (see Fig. 1).

To illustrate frequency linearity and potential *versus* current equivalence, we used a mixture of four different sine wave frequencies at different amplitudes in different simulated scalp locations. We identified each simulated scalp sensor by its spectrum using the following convention: beta frequencies of 16 Hz and 20 Hz with maximum amplitudes in the anterior electrodes (F7 and F8) and alpha frequencies 8 Hz and 10 Hz with maximum amplitudes in the posterior electrodes (O1 and O2). As shown in Figure 1 the lower beta and alpha frequencies of 16 Hz and 8 Hz were located in the right hemisphere and the higher beta and alpha frequencies of 20 Hz and 10 Hz were located in the left hemisphere. In the same way, a frequency shift toward the lower frequencies was located in the right hemisphere. The sine wave mixtures were computed using two different base frequencies 8 Hz and 10 Hz that for some electrode sensors were doubled in frequency, *i.e.*, 16 Hz and 20 Hz and/or doubled in amplitude:

$$S(i,j) = A\,i \sin(2\pi j \alpha i) + B\,i \sin(2\pi j \beta i) \tag{5}$$

where $\beta i = 2\alpha i$ and $S(i,j)$ is the value of the signal in the sensor closest to the source i where i is the odd numbered sources and j is the time-sample (1024 time samples total). The amplitude of the lower

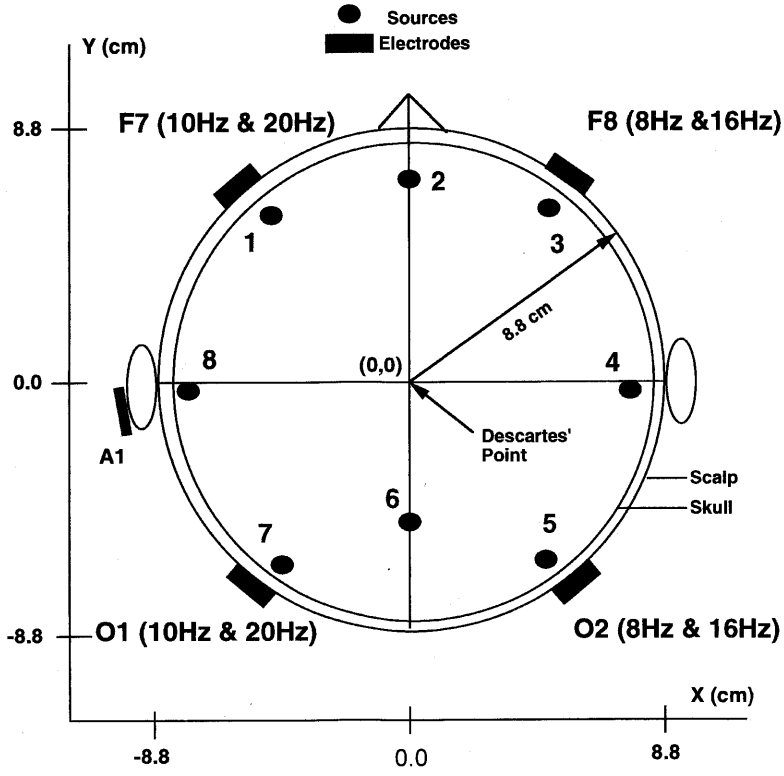

FIGURE 1 The three-Shell spherical model of the head used to simulate LORETA. Four electrodes (F7 F8 O1 O2) and the reference electrode (A1) are indicated by black rectangles. The coordinates of the electrodes are according to the best-fitting sphere relative to cortical anatomy (Towel *et al.*, 1993). The peaks of beta (for F7 and F8) and alpha activity (for O1 and O2) are indicated in parenthesis. Eight sources (1 to 8) indicated by black circles were located in the interior of the sphere to represent the equivalent current sources such as in the gray matter.

frequencies (Ai) is related to the amplitude of the higher frequencies (Bi):

$$Ai = Bi/2 = 5\text{V}, \text{ for } i = 1, 3(\text{F7}, \text{F8}) \tag{6}$$

$$Ai = 2Bi = 10\text{V}, \text{ for } i = 5, 7(\text{O1}, \text{O2}) \tag{7}$$

The Fourier-spectra of the electrodes are shown at the left side of Figure 2. The results of applying the Fast Fourier Transform (FFT) to the time series recorded at the sensors and then computing the inverse

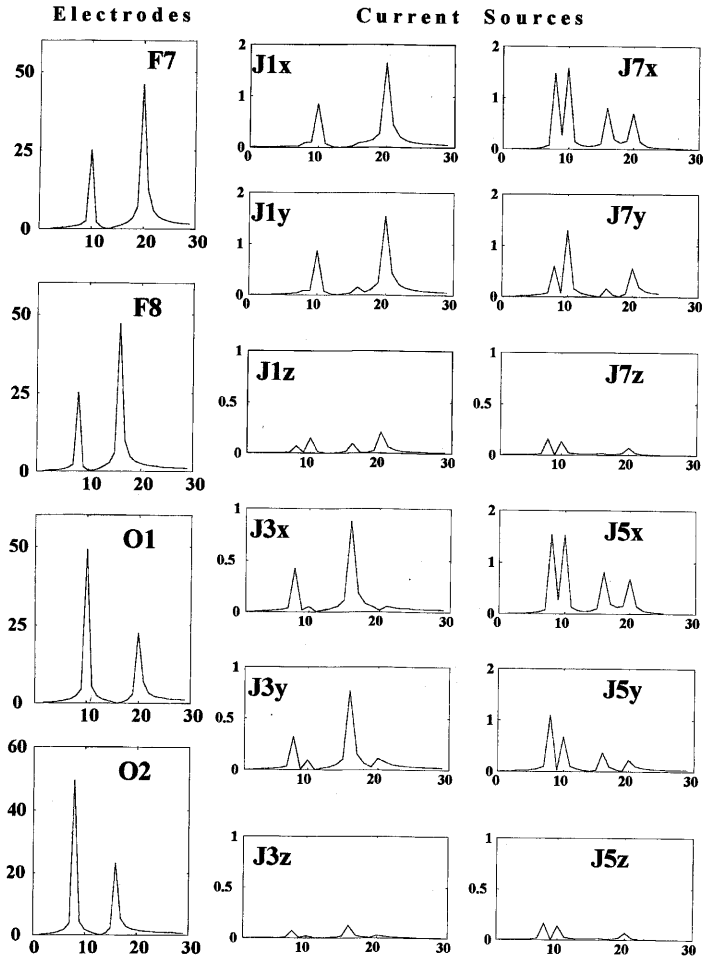

FIGURE 2 Power Spectrum of the signals used to simulate LORETA. The spectrum of the signals in the scalp electrodes is shown on the left (amplitude of beta is higher in the anterior regions, alpha amplitude is higher in the posterior regions and a frequency shift toward the lower frequencies is in the right hemisphere). The center and right columns are the spectra of the current sources nearest to the electrodes J1, J3, J5 and J7 after calculating the inverse solution. Each source has three components x, y and z. The y-axis of the electrodes is uv^2/cycle/sec for the electrodes and $(uA/cm^2)^2$/cycle/sec for current density at each source location. The x-axis is frequency in Hz in all cases. This simulation confirms the mathematical statements and demonstrates a frequency domain equivalence between the spectra of electrical potentials at the scalp and the spectra of currents in the interior of the head model.

solution to obtain the simulated currents are shown at the right of Figure 2. The same spectrum was obtained when we apply first the inverse solution and then the FFT. Thus, the first method represents a considerable simplification of the application of the FFT to the sources since there are a total of 24 current sources and only four scalp sensor locations.

It can be seen in Figure 2 that as a consequence of the linearity of the model, no new frequency is created and the same Fourier components are present in the current sources as in the scalp potential. The z components of the current spectra were very small because all of the points shown in Figure 1 were in the same z plane. An interesting effect is that the sequence observed in the frequency peaks can be related with the distance between the source and the electrode, but this is not always exactly the case such as in J7x where the 16 Hz component is larger than the 20 Hz component. These effects, as well as the capacity of LORETA to localize deep sources reflect the special benefits of applying the smoothness criteria. Consequently, the search in the solution space is not always choosing the obvious solutions but the more physiological (Pascual-Marqui, 1994; Anderer *et al.*, 1998a, 1998b; John *et al.*, 1998; Saletu *et al.*, 1998; Llinas, 1988; Strik *et al.*, 1998; Lantz, 1997).

4. DISCUSSION

We have applied the inverse solution ($J = TS$) (where J is the current density, T is a generalized inverse and S is the electrical or magnetic signal) first and then the Fourier transform to the sources (FFT(J)) and we compared this result to what is obtained when we apply the Fourier transform to the potentials and then the inverse solution $\mathrm{FFT}(J) = T^{*}\mathrm{FFT}(S)$. The spectrum obtained from the magnitude of the real and imaginary part of the Fourier transform was demonstrated mathematically and in simulations to be equivalent, *i.e.*:

$$\mathrm{abs}(\mathrm{FFT}(T \cdot S)) = \mathrm{abs}(T \cdot \mathrm{FFT}(S))$$

Improving the localization accuracy of the frequency of the EEG/MEG can be accomplished not only by co-registration with a structural modality such as MRI but also with co-registration with another

functional technique. In this way, an EEG-derived time series is computed for each of the MRI and PET validated dipoles using a pseudoinverse method (Thatcher *et al.*, 1994; Thatcher, 1995).

Biophysical linkages between EEG-parameters (amplitude, current density, frequency, coherence and phase) and the MRI-based structure of brain tissues has been explored (Thatcher *et al.*, 1998a, 1998b, 1999). In these studies it has been shown that 3-dimensional quantitative analysis of T2 relaxation times can also be used to constrain the solution space of the sources. In this way, the scalar and vector values of MRI T2 relaxation times as well as different frequency sources inside the brain may be used to improve the speed and accuracy of source localization.

The results of this paper emphasizes that an additional improvement can be accomplished when one applies frequency domain analysis. In this case, the frequency itself may reflect preferential oscillatory modes (Gomez and Lopera, 1999). For example, it is generally recognized that there is a positive co-relation between rCBF (regional cerebral blood flow), metabolic changes and electrical activity (Steriade *et al.*, 1990). Normally, the higher the frequency, the higher the rCBF. rCBF can be detected by PET or fMRI and thus the search space of high frequency dipole sources can be limited to those spaces suggested by the PET, fMRI and biophysical measures from the MRI (Thatcher *et al.*, 1994, 1999).

Acknowledgement

This project was supported by contract no. JFC36285006 as part of the Department of Defense and Veterans Head Injury Program (DVHIP).

References

Anderer, P., Pascual-Marqui, R., Semlitsch, V. & Saletu, B. (1998a) Differential effects of normal aging on sources of standard N1, target N1 and target P300 auditory event-related brain potentials revealed by low resolution electromagnetic tomography (LORETA). *Electroenceph. Clin. Neurophysiol.*, **108**, 160–174.

Anderer, P., Pascual-Marqui, R., Semlitsch, V. & Saletu, B. (1998b) Electrical Sources of P300 Event-Related Brain Potentials Revealed by Low Resolution Electromagnetic Tomography. *Pharmacopsychiatry*, **37**, 20–27.

Baillet, S. & Garnero, L. (1997) A Bayesian Approach to Introducing Anatomo-Functional Priors in the EEG/MEG Inverse Problem. *IEEE Trans. Biomed. Eng.*, **44**(5), 374–385.

Gomez, J. F. & Lopera, F. L. (1999) A topological hypothesis for the functional connections of the cortex. A principle of the cortical graphs based on neuroimaging. *Medical Hypotheses*, **53**(3), 263–266, 1999.

Handerson, E., Butler, S. R. & Glass, A. (1975) The Localization of equivalent dipoles of EEG sources by the application of electrical field theory. *Electroencephal. Clin. Neurophysiol.*, **79**, 119–130.

John, E. R., Prichep, L. S., di Michele, F. & Valdes Sosa, P. (1998) Loreta images of QEEG subtypes of psychiatric disorders with differential treatment responsiveness. *Brain Topography*, **11**(1).

Lagerlund, T., Sharbrough, F., Jack, C., Erickson, B., Strelow, D., Cicora, K. & Busacker, N. (1993) Determination of 10-20 system electrode locations using magnetic resonance image scanning with markers. *Electroencephal. Clin. Neurophysiol.*, **86**, 7–14.

Lantz, G., Michel, C., Pascual Marqui, R., Spinelli, L., Seeck, M., Seri, S., Landis, T. & Rosen, I. (1997) Extracranial localization of intracranial interictial epileptiform activity using LORETA (low resolution electromagnetic tomography) *Electroencephal. Clin. Neurophysiol.*, **102**, 414–422.

Llinas, R. R. (1988) The intrinsic electrophysiological properties of mammalian neurons: insights into the central nervous system function. *Science*, **242**, 1654–1664.

Malmivuo, J. & Plonsey, R. (1995) *Bioelectromagnetism*, New York, Oxford University Press.

Menke, W. (1984) *Gephysical Data Analysis*: *Discrete Inverse Theory*. Orlando: Academic Press.

Pascual-Marqui, R.-D., Michel, C. M. & Lehman, D. (1994a) Low Resolution Electromagnetic Tomography: A New Method for Localizing Electrical Activity in the Brain. *Int. Journal of Psychophys.*, **18**, 49–65.

Pascual Marqui, R. (1994b) Low Resolution Electromagnetic Tomography. *Brain Topography*. **7**, 180 (Abstract) The seventh Swiss brain mapping meeting, Zurich, March.

Saletu, B., Anderer, P. & Pascual-Marqui, R. D. (1998) LORETA after representative drugs of the main psychopharmacological classes. *Brain Topography*, **11**(1), 71–80.

Strik, W. K., Fallgatter, A., Brandeis, D. & Pascual-Marqui, R. (1998) *Three dimensional tomography of event related potentials during response inhibition*: *evidence for phasic frontal lobe activation.*

Steriade, M. *et al.* (1990) Basic Mechanisms of Cerebral Rhythmic Activities. *Electroencephal. and Clin. Neurophysiol.*, **76**, 481–508.

Thatcher, R. W. & John, E. R. (1977) *Functional Neuroscience*, **1**, Foundations of Cognitive Processes. L. Erlbaum Assoc., N.J.

Thatcher, R. W., Wang, B., Toro, C. & Hallett, M. (1994) Human Neural Networks Dynamics Using Multimodal Registration of EEG, PET, and MRI. In: Thatcher, R., Hallett, M., Zeffiro, T., John, E. and Huerta, M. (Eds.), *Functional Neuroimaging*: *I- Technical Foundations*, Academic Press: New York.

Thatcher, R. W. (1995) Tomographic EEG/MEG. *Journal of Neuroimaging*. **5**, 35–45.

Thatcher, R. W., Biver, C., Camacho, M., McAlaster, R. & Salazar, A. M. (1998a) Biophysical linkage between MRI and EEG amplitude in traumatic brain injury. *NeuroImage*, **7**, 352–367.

Thatcher, R. W., Biver, C., McAlaster, R. & Salazar, A. M. (1998b) Biophysical linkage between MRI and EEG coherence in traumatic brain injury. *NeuroImage*, **8**(4), 307–326.

Thatcher, R. W., Biver, C., Gomez, M. & Salazar, A. M. (1999) 3-Dimensional vector analysis of MRI relaxometry and current source localization (LORETA) of EEG in traumatic brain injury. *Neuroimage*, **9**(6), S110.

Toro, C., Wang, B., Zeffiro, T., Thatcher, R. W. & Hallett, M. (1994) Cortical activation accompaning self-paced finger movements: Integration of equivalent dipole sources with MR and PET images. In: Thatcher, R., Hallett, M., Zeffiro, T., John, E. and Huerta, M. (Eds.), *Functional Neuroimaging: I-Technical Foundations*, Academic Press: New York.

Towle, V., Bolaños, J., Suarez, D., Tam, K., Grzeszczuk, R., Levin, D., Cakmur, R., Frank, S. & Spire, J. (1993) The spatial location of EEG electrodes: locating the best-fitting sphere relative to cortical anatomy: *Electroencephal. Clin. Neurophysiol.*, **86**, 1–6.

Valdes, P. (1997) Quantitative electroencephalographic tomography. *EEG Clin. Neurophysiol.*, **103**, 19.

Valdes, P., Bosch, J., Virues, T., Aubert, E., Fermin, E. & Gonzalez, E. (1998) EEG source frequency domain SPM, *Neuroimage*, S636.